Measurement Science
and Technology

PAPER • OPEN ACCESS

Determination of electromagnetic shielding effectiveness using an enhanced Absorber Box method: theoretical, simulation, and experimental approaches

To cite this article: Andrea Amaro *et al* 2025 *Meas. Sci. Technol.* **36** 076003

OPEN ACCESS
IOP Publishing
Measurement Science and Technology
Meas. Sci. Technol. 36 (2025) 076003 (14pp)
https://doi.org/10.1088/1361-6501/ade55a

Determination of electromagnetic shielding effectiveness using an enhanced Absorber Box method: theoretical, simulation, and experimental approaches

Andrea Amaro[1,*], Jose Torres[1], Adrian Suarez[1], Roberto Herraiz[1], Pedro A Martinez[1], Jesús Soret[1], Raimundo Garcia-Olcina[1] and Antonio Alcarria[2]

[1] Department of Electronic Engineering, University of Valencia, 46100 Valencia, Spain
[2] EMC Shielding & Grounding Team, Würth Elektronik eiSos, 74638 Waldenburg, Germany

E-mail: andrea.amaro@uv.es

Received 9 April 2025, revised 3 June 2025
Accepted for publication 17 June 2025
Published 25 June 2025

Abstract
Accurate characterization of shielding effectiveness (SE) is essential for evaluating electromagnetic interference shielding materials in high-frequency applications such as 5G communications, automotive, radar, and aerospace. Standardized methods like ASTM D4935-18 and IEEE 299-2006 have frequency limitations, precise sample preparation, and demand complex experimental setups that can hinder practical implementation. This study presents an advanced characterization of an optimized Absorber Box methodology that enhances SE measurement accuracy, extends the frequency range beyond 1.5 GHz, and minimizes edge diffraction effects. The proposed approach provides a controlled testing environment in a more compact setup compared to anechoic chambers, facilitating practical implementation without compromising precision. The system's reliability is validated through numerical simulations using finite element method analysis. Experimental results confirm the method's ability to differentiate materials with different SE, demonstrating strong agreement between simulated and measured data. This approach offers a flexible and robust alternative to conventional SE measurement techniques, making it particularly advantageous for high-frequency shielding material characterization.

Keywords: electromagnetic shielding, Absorber Box, finite element method, shielding effectiveness, EMI characterization

* Author to whom any correspondence should be addressed.

1. Introduction

The characterization of electromagnetic shielding materials has become a fundamental aspect of electromagnetic compatibility (EMC) research due to the growing complexity of electronic systems and the increasing prevalence of high-frequency electromagnetic interference (EMI) [1, 2].

The rapid expansion of 5G technology, which operates across both the sub-6 GHz and millimeter-wave frequency bands, has significantly heightened concerns about EMI, as wireless communication, automotive radar, aerospace electronics, and industrial applications demand robust shielding solutions [3, 4]. Effective electromagnetic shielding is critical for ensuring system reliability, reducing signal degradation, and preventing interference between components in densely packed electronic environments. Given these challenges, accurate measurement techniques are essential for evaluating the shielding effectiveness (SE) of materials, particularly at high frequencies where standard methods face significant limitations [5].

Standardized methods for measuring SE, such as ASTM D4935-18 and IEEE 299-2006, provide well-established frameworks for evaluating electromagnetic shielding performance [6, 7]. However, these methods present limitations that can hinder their applicability in specific measurement scenarios. The assumptions and conditions under which these standards were originally developed may not always align with the characteristics of emerging shielding materials or novel application contexts.

As shielding technologies continue to evolve, these constraints highlight the need for alternative methodologies that offer greater flexibility and adaptability to modern measurement requirements.

One of the main constraints of ASTM D4935-18 is its restricted frequency range, which is inherently limited by the coaxial transmission line geometry to frequencies below approximately 1.5 GHz. This frequency limit renders ASTM D4935-18 inadequate for assessing materials intended for millimeter-wave 5G systems, where adapted measurement techniques are required to evaluate frequency-dependent shielding materials [8]. Furthermore, this method needs precise circular sample geometries, typically of rigid or uniform composition, which are incompatible with flexible, non-homogeneous, or nanostructured materials frequently encountered in novel EMI shielding solutions.

On the other hand, IEEE 299-2006 offers broader frequency coverage through free-space measurement techniques, but its implementation introduces significant practical challenges. The method requires large planar samples or shielding enclosures and typically requires specialized anechoic chambers, limiting its accessibility for researchers without such infrastructure. Moreover, although sometimes applied to individual material samples, this standard is primarily intended to evaluate complete shielding enclosures, reducing its suitability for early-stage material screening or miniaturized applications.

In both cases, traditional techniques often face limitations when dealing with specific sample geometries, especially when these are difficult to implement with certain materials, due to limited material availability or budget constraints, which are common in developing advanced shielding materials. All these factors underscore the need for compact, cost-effective, and versatile alternatives, such as the improved Absorber Box methodology proposed in this study, which maintains measurement accuracy while adapting to research aligned with current industrial realities.

Many modern materials, such as nanocomposites, flexible shielding films, and metamaterials, do not conform to the strict geometrical and dimensional requirements imposed by the standards. These materials often exhibit non-uniform compositions, unconventional thicknesses, or structural characteristics that hinder their compatibility with traditional testing setups [9–11]. In response, alternative SE measurement techniques have emerged, offering more flexible and adaptable approaches that accommodate a wider variety of material configurations [12]. These alternatives enable the accurate characterization of novel shielding solutions while addressing the geometric and environmental constraints that standard methods may impose [13–16].

Among these emerging approaches, Absorber Box-based methodologies have proven to be a promising alternative for SE measurement [17]. By providing a controlled electromagnetic environment, Absorber Box effectively reduces external interferences, minimizes environmental variability, and offers greater flexibility in sample preparation. These characteristics make them particularly well-suited for evaluating shielding materials across a broad frequency spectrum while maintaining measurement reliability and reproducibility [16, 18, 19]. These systems are particularly advantageous when characterizing materials in the gigahertz frequency range, where conventional techniques struggle with precision due to their inherent design limitations.

However, despite their advantages, traditional Absorber Box methods present certain limitations. One of the most significant challenges encountered in these setups is the edge diffraction effect, a phenomenon that occurs when electromagnetic waves interact with the boundaries of the sample of the material under test (MUT), leading to diffraction, scattering, and potential leakage of energy [20, 21]. The impact of this effect depends on factors such as the wavelength of the incident wave, the size and shape of the sample, and the configuration of the Absorber Box. At frequencies where wavelengths become comparable to the sample dimensions, edge diffraction effects can introduce measurement inaccuracies, leading to over or underestimation of its shielding performance.

This study presents a comprehensive study of an enhanced Absorber Box methodology incorporating modifications designed to improve measurement accuracy and optimize key parameters, such as antenna distance and sample size, to minimize diffraction effects. By refining the sample holder configuration and ensuring a more uniform electromagnetic field distribution within the measurement cavity, this approach enhances the precision of SE evaluations over a broader frequency spectrum. Additionally, it extends the measurement capabilities beyond 1.5 GHz, addressing high-frequency requirements for emerging EMI shielding applications. The system features a custom-fabricated, fully enclosed metallic structure without structural slots or seams, eliminating leakage paths and improving field confinement. Internally, multilayer microwave absorbers are placed to suppress internal reflections and stabilize wave propagation. The design also allows modular and reproducible antenna placement, supporting consistent measurement geometry without physical modifications. These improvements directly address the main limitations of standardized methods such as ASTM D4935-18, which is restricted in frequency and geometry, and IEEE 299-2006, which requires large anechoic chambers and full enclosure testing. To validate the proposed approach, ANSYS HFSS, a widely used 3D finite element method (FEM) analysis tool, is employed to create a digital twin of the measurement system, enabling predictive analysis and iterative optimization. Numerical simulations provide a detailed assessment of electromagnetic wave interactions with shielding materials, facilitating the identification of potential sources of error before experimental testing. By comparing simulated results with experimental data, this study ensures measurement accuracy and reliability while refining key system parameters for enhanced precision.

The manuscript is structured as follows: first, the experimental methodology is described, detailing the modifications introduced to enhance measurement accuracy and minimize the edge diffraction effect. Next, the simulation framework developed using FEM analysis is outlined, illustrating how computational modeling is used to refine the measurement setup and predict shielding behavior. Subsequently, experimental results are presented and compared with simulation predictions, demonstrating the effectiveness of the proposed method in characterizing high-frequency shielding materials. Finally, the conclusions summarize the key findings of the study, emphasizing the broader implications of the enhanced measurement approach in the field of electromagnetic shielding, highlighting, the capability of the absorber-based system to measure materials with different SE levels and differentiate them with precision and reliability.

2. Measurement method

Ensuring accurate and reproducible evaluation of SE requires a well-defined measurement setup that minimizes external interferences and maintains consistency across experiments. This study employs a structured enclosure to achieve these objectives, providing a controlled environment for electromagnetic characterization.

The measurement system is enclosed within a 50 × 50 × 50 cm metal enclosure. This design provides flexibility in experimental configurations, allowing for precise control over the distance between antennas and accommodating larger samples. The cubic geometry ensures a directional electromagnetic field distribution within the cavity, minimizing measurement inconsistencies that may arise from asymmetric boundary conditions. Furthermore, the enclosure's dimensions enhance the system's versatility, enabling compatibility with a broader range of materials and facilitating more comprehensive evaluations of SE. These design considerations contribute to a controlled and reproducible measurement environment, improving accuracy in electromagnetic characterization.

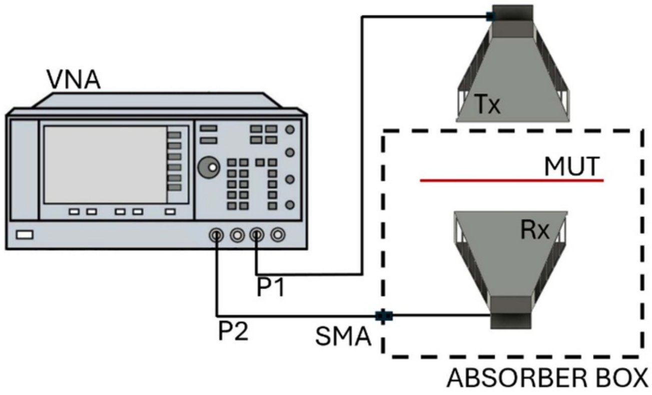

Figure 1. Schematic of the Absorber Box measurement setup.

2.1. Evaluation of the new approach: Absorber Box method

This study proposes a substantial improvement over the previous design of the measurement box by modifying its dimensions to 50 × 50 × 50 cm. In conventional designs, the presence of slots in the structure of the box can generate slot-antenna effects, leading to electromagnetic field leakage and affecting measurement accuracy [22]. In the current version, the enclosure was fabricated by a specialized metalworking company using folded aluminum panels with welded edges, resulting in a continuous metallic surface with no structural slots. A single SMA port was included for the receiving antenna cable, carefully sized to minimize leakage. This optimization of the cavity dimensions promotes a more homogeneous distribution of the electromagnetic field inside, allowing for directional signal propagation and reducing unwanted reflections that could affect the measurement.

The measurement procedure is carried out using a 26.5 GHz Keysight P9375A vector network analyzer (VNA). For the experimental setup shown in figure 1, port 1 of the VNA is connected to the transmitting antenna, located outside the box. The receiving antenna, positioned inside the cavity, is connected to a coaxial cable with an SMA connector that passes through the box via a drilled hole, establishing the connection with port 2 of the VNA. This configuration enables accurate characterization of the samples, ensuring reliable and reproducible measurements.

Multilayer foam absorbent materials with a thickness of 25 mm and dimensions of 50 × 50 cm have been used to minimize internal reflections and ensure that electromagnetic waves are properly attenuated within the box. These absorbers, based on carbon-loaded polyurethane foam (TFAL-Series), are laminated to produce a graded conductivity profile suitable for broadband operation [23]. They have been cut and arranged to match the geometry of the receiving antenna. Additionally, by adjusting the number of absorber layers placed inside the cavity, the effective distance between the antennas can be modified, allowing different configurations to be studied without altering the physical structure of the box.

Subsequently, the SE (dB) of the sample is calculated according to equation (1):

$$\text{SE (dB)} = \text{S21}_{\text{sample}} - \text{S21}_{\text{ref}} \quad (1)$$

where S21_{ref} is the transmission parameter of the air measured between the two antennas without any sample, and $\text{S21}_{\text{sample}}$ is the transmission parameter of the sample placed between the antennas.

Thanks to this optimized design, the proposed system enables accurate measurements while avoiding errors caused by signal dispersion or external interference. One of its key advantages is that it eliminates the need for an anechoic chamber, allowing measurements to be performed in a compact space without requiring large-scale setups. Additionally, this system does not necessitate large material samples, as measurements can be conducted with samples only a few centimeters in size. This is particularly beneficial for evaluating expensive or difficult-to-manufacture materials, where minimizing sample size in testing stages is essential for cost efficiency and practicality. The reduced space requirements and the simplicity of the experimental configuration also contribute to a lower overall measurement cost, as the setup can be deployed in standard laboratory environments without the need for specialized infrastructure. Compared to traditional methods, the enhanced Absorber Box offers a portable and accessible alternative that enables rapid and repeatable evaluations, making it suitable for iterative testing, early-stage material screening, or comparative studies across a wide frequency range.

This approach represents a significant advancement in the characterization of materials and electromagnetic devices, providing a robust and reproducible method for evaluating electromagnetic properties in a controlled measurement environment. Furthermore, this system allows easy and efficient sample measurement, facilitating its use in various research and development applications.

The final experimental system is shown in figure 2, where the emitting horn antenna is situated above a MUT and connected to the VNA equipment.

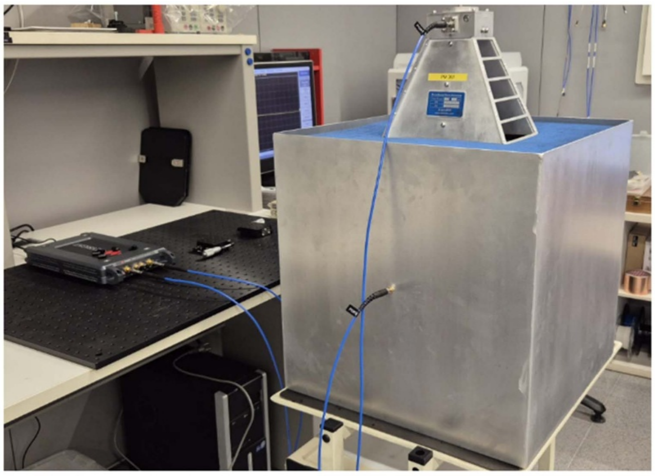

Figure 2. Configuration of the real experimental system: Absorber Box.

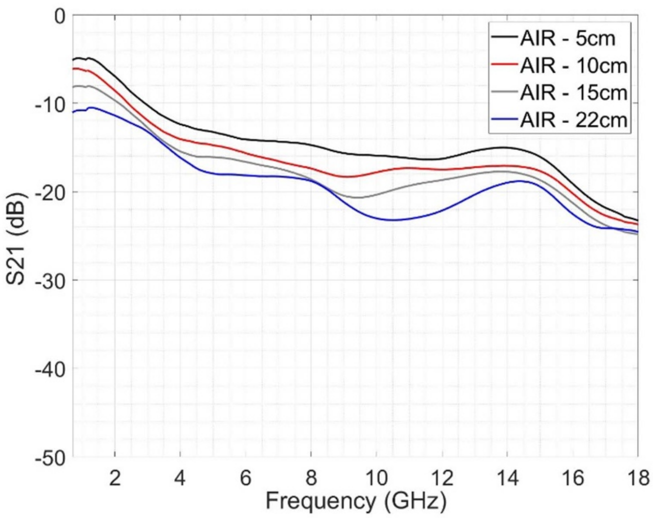

Figure 3. Air S_{21} parameter between the antennas varying the distance.

2.2. Characterization of the Absorber Box method

To ensure the reliability and reproducibility of the measurements in the experimental system, preliminary tests of the S_{21} parameter in air were carried out by varying the separation between the transmitting and receiving antenna. Distances of 5 cm, 10 cm, 15 cm and 22 cm were tested, the results of which are presented in figure 3.

The analysis of the data obtained reveals that there is a relationship between the transmission coefficient S_{21} and the distance between the antennas following a behavior that, under far-field conditions, is described by the Friis transmission equation [24]:

$$P_r = P_t \left(\frac{\lambda}{4\pi d}\right)^2 G_t G_r \quad (2)$$

$$S_{21} = 10\log_{10}\left(\frac{P_r}{P_t}\right) = 10\log_{10}\left[\left(\frac{\lambda}{4\pi d}\right)^2 G_t G_r\right] \quad (3)$$

where P_r represents the received power, P_t is the transmitted power, λ is the wavelength, d is the separation between antennas, and G_t and G_r are the gains of the transmitting and receiving antennas, respectively. This equation highlights the inverse square dependence of received power on distance, which explains the observed attenuation trend in the experimental data.

However, in our case, the antenna separations place the system in a regime where the far-field condition, typically defined as $d \gg 2D^2/\lambda$, is not satisfied, preventing the direct application of the Friis equation, which assumes far-field propagation. Nevertheless, while near-field effects such as reflections and diffraction could introduce additional complexities, these are mitigated by the absorbers used inside the cavity and the sample size, an aspect that is analyzed in detail later in this work. The use of absorbing materials within the cavity represents a controlled environment, minimizing reflected waves and multipath propagation, which could otherwise affect the near-field measurement accuracy.

Therefore, since the theoretical model cannot be directly applied in this case, we adopt a balanced approach that combines experimental reference measurements and numerical simulations. Specifically, we use the S_{21} measurement of the air between the two antennas as an experimental reference, which serves as a baseline for comparison. Additionally, a simulation model of the system will be developed in ANSYS HFSS to validate the measurement setup and ensure consistency between experimental results and theoretical expectations within the considered distance regime.

As shown in figure 3, the measured S_{21} parameter decreases as the antenna separation increases, following the theoretical free-space path loss model. Notably, the attenuation becomes more pronounced for distances greater than 10 cm, particularly at frequencies above 6 GHz, where the signal reduction is significant. This behavior is consistent with the wavelength dependence, as higher frequencies correspond to shorter wavelengths, leading to increased propagation losses. Additionally, at larger distances, diffraction effects and multipath interference become more relevant, causing fluctuations in the received signal and compromising measurement stability.

Based on these results, a distance of 5 cm was established as the optimum condition for the measurements in this study. This configuration provides an adequate balance between efficiency in signal transmission and reduction of external disturbances, thus minimizing the introduction of systematic errors in the characterization of the samples. In this way, a controlled and reproducible experimental framework is guaranteed, which allows for obtaining reliable and representative results in analyzing the S_{21} parameter.

Once the optimal measurement distance was established, an analysis was conducted to evaluate the influence of sample size on SE. For this purpose, copper foil (EMC shielding tape) with a thickness of 0.04 mm was used, varying its dimensions as shown in figure 4. This analysis aims to determine how different sample sizes affect the measured attenuation across the frequency range, ensuring that the SE characterization remains consistent and reliable.

The results obtained from the measurement of samples of different copper foil sizes with the Absorber Box measurement method are presented in figure 5. The results reveal a clear dependence of the SE on the dimensions of the sample. Specifically, larger samples show higher attenuation levels across the entire frequency range, with values below −40 dB, even the largest samples showing attenuations below −80 dB. In contrast, as the sample size decreases, the SE performance is quite affected, decreasing to values of −10 dB for the smallest sample of 12 × 12 cm. This trend is particularly evident at lower frequencies, where the differences in SE become more pronounced.

One of the main factors influencing electromagnetic shielding measurements is the edge diffraction effect. In this phenomenon, an incident wave interacts with the boundaries of a

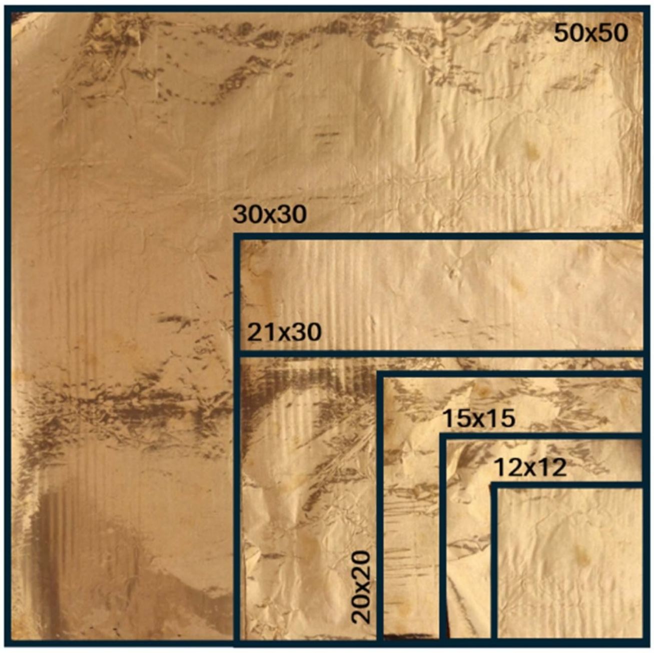

Figure 4. Copper foil (EMC shielding tape) samples of various dimensions.

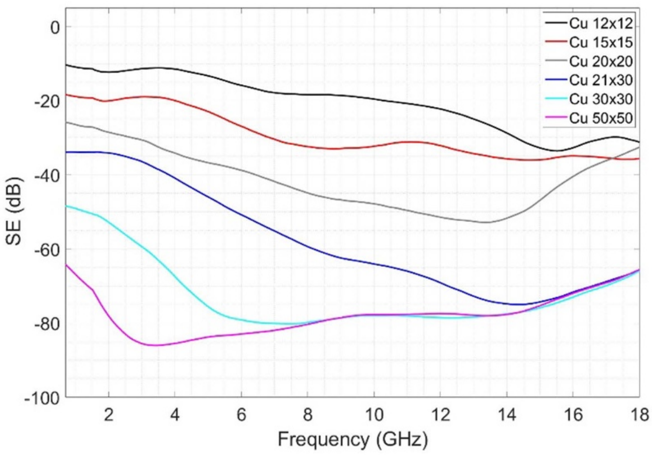

Figure 5. SE of the copper foil, varying the sample size.

conductive sample, leading to energy leakage beyond the geometric shadow region. When an electromagnetic wave encounters a discontinuity, such as the sharp edges of a conductive sheet, part of the energy is scattered in different directions, contributing to diffraction losses. The extent of diffraction depends on the relationship between the sample size (L) and the wavelength (λ):

1. If $L \gg \lambda$: the diffraction effect is less significant.
2. If $L \ll \lambda$: the diffraction effect is more significant.

In our specific case, the frequency range spans from 700 MHz to 18 GHz, corresponding to wavelengths ranging from approximately 42.8 cm (at 700 MHz) to 1.67 cm (at 18 GHz). Since the sample dimensions in our setup are on the order of tens of centimeters, diffraction effects are more pronounced at lower frequencies where $L \ll \lambda$, leading to significant energy leakage beyond the geometric shadow region. As the frequency increases ($L \gg \lambda$), the diffraction effect becomes less significant, improving measurement accuracy. This behavior underscores the need for an optimized measurement configuration to mitigate diffraction-related errors, particularly in the lower-frequency range.

From an analytical perspective, the diffraction coefficient D_{UTD} quantifies the fraction of the electromagnetic wave that bends around the edges of a conducting sheet. This coefficient is derived from the uniform theory of diffraction (UTD), which extends the geometrical theory of diffraction to provide a more accurate description of wave propagation near discontinuities.

The diffraction coefficient is expressed as:

$$D = \frac{e^{\frac{j\pi}{4}} \sin\frac{\pi}{n}}{n(2\pi k)^{1/2} \sin\beta} \left[\left(\cos\frac{\pi}{n} - \cos\frac{\theta - \alpha}{n} \right)^{-1} \mp \left(\cos\frac{\pi}{n} - \cos\frac{\theta + \alpha + \pi}{n} \right)^{-1} \right] \quad (4)$$

where $k = \frac{2\pi f}{c}$ is the wavenumber, $n = \frac{\pi}{\alpha}$ is the wedge parameter determined by the internal angle α, θ represents the incident wave angle, and β is the diffraction angle [25–27].

In the specific case of the experimental setup considered, where the incident wave is normal to the sample ($\theta = 0°$), the diffraction wave propagates perpendicularly to the plane ($\beta = 90°$), and the distance between the antennas and the sheet is small compared to the sample size ($r_1 \approx r_2 \ll L$), the diffraction effect is primarily governed by the sample dimensions rather than the distance between the antennas [28]. Under these conditions, the diffraction coefficient simplifies to:

$$D_{\text{UTD}} \approx \frac{e^{\frac{-j\pi}{4}}}{\sqrt{2\pi kL}}. \quad (5)$$

This expression reveals two fundamental characteristics of the diffraction process. First, as the size of the sheet increases, the diffraction effect diminishes since a larger sheet obstructs wave propagation more effectively, reducing the amount of energy diffracted beyond the geometric shadow region. Second, at lower frequencies, diffraction losses become more pronounced as longer wavelengths interact more significantly with obstacles and tend to bend around edges more easily. Consequently, at higher frequencies, the diffraction effect is less significant, which increases the shielding performance of the sample. This relationship underscores the importance of considering diffraction effects when evaluating SE, particularly for finite-sized samples, as they can introduce measurement uncertainties that may lead to overestimating transmission losses if not properly accounted for.

From an experimental standpoint, as illustrated in figure 5, edge diffraction effects significantly influence the SE of the samples. In smaller samples, the interaction between the incident electromagnetic waves and the sample boundaries enhances diffraction, increasing wave leakage and consequently reducing the overall shielding performance. This effect is particularly noticeable at lower frequencies, where the wavelength is comparable to the characteristic dimensions of the sample, leading to a greater contribution of diffracted energy to the transmitted field. A key observation is that the SE curves for the 50 × 50 cm and 30 × 30 cm samples converge in the 7–8 GHz frequency range, indicating that diffraction effects become negligible beyond a specific sample size and shielding performance stabilizes. In this range, the wavelength becomes small compared to the sample size, reducing the relative influence of edge diffraction. In this frequency band, the shielding behavior stabilizes, and the attenuation is mainly governed by the material's intrinsic properties, rather than by geometric constraints. This suggests that increasing the sample size beyond this point does not significantly enhance SE, as the measured attenuation is primarily governed by the intrinsic properties of the material rather than by geometric constraints. Furthermore, larger samples exhibit a smoother attenuation trend across the frequency range, whereas smaller samples present more pronounced variations. This indicates that edge diffraction not only reduces SE but also introduces fluctuations in the measured values. These variations may affect the accuracy of the characterization, underscoring the importance of selecting an appropriate sample size to obtain reliable and reproducible results.

These findings highlight the necessity of optimizing sample dimensions to achieve meaningful SE measurements. The sample size should be large enough to minimize diffraction-related losses while ensuring that the measured SE corresponds to the material's inherent behavior. To achieve representative results, it is advisable to use sample dimensions larger than the dominant wavelengths within the analyzed frequency range. This minimizes edge diffraction effects and ensures a more accurate evaluation of the shielding performance.

Based on these results, it is concluded that, for this system, the optimal sample size corresponds to the maximum cavity dimensions, 50 × 50 cm. However, due to practical limitations related to the standard dimensions of commercially available materials, 30 × 30 cm samples will be used in this study. Given that the SE traces for 30 × 30 cm and 50 × 50 cm converge at 7–8 GHz, these frequencies will be considered as the threshold above which diffraction effects no longer influence the SE values. By focusing the analysis on frequencies above this limit, a more precise characterization of the SE can be achieved, ensuring that the measured values reflect the intrinsic properties of the material rather than being affected by edge-related phenomena.

3. Simulation model definition

In this study, a FEM simulation model was developed to validate the behavior of the real system. The primary objective of the model is to serve as a 'digital twin' of the physical setup, allowing for a detailed analysis of the system's performance under various conditions. By recreating the real-world configuration as accurately as possible, this model allows for detailed simulations that predict the system's behavior and assist in optimizing its design.

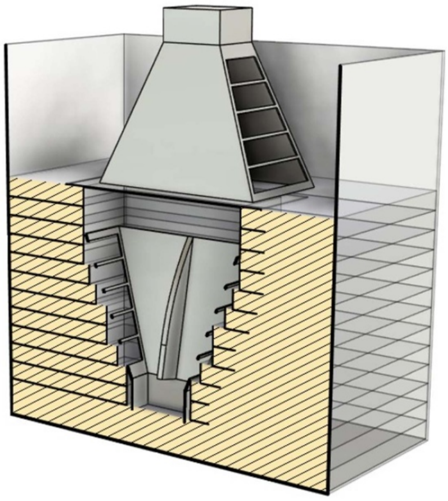

Figure 6. 3D model of the Absorber Box method with a sample under test.

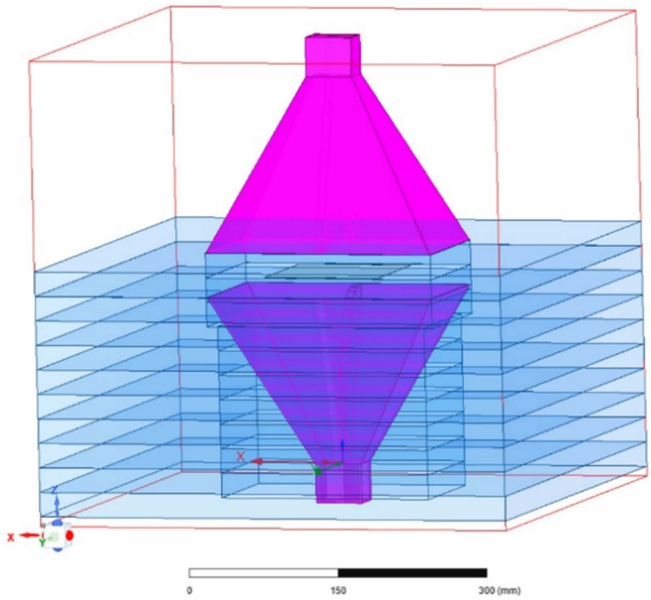

Figure 7. Simulation model of the Absorber Box method.

The FEM simulation is created using the software ANSYS HFSS Electronics Desktop. The experimental measurement setup has been replicated to assess the scattering parameter S_{21} of the developed system. To accurately simulate the full-scale system, broadband antennas were carefully designed and validated to replicate the performance of real antennas within the frequency range of 0.7–18 GHz. These antennas are excited using wave ports to ensure precise electromagnetic field excitation. The mesh density was optimized in both the antennas and the sample under test to achieve reliable and convergent simulation results. Additionally, the electromagnetic properties of the microwave-absorbing material used to line the interior of the enclosure were obtained directly from the manufacturer, ensuring accurate modeling of wave absorption characteristics. The enclosure walls were modeled using perfect electric conductor boundary conditions, while impedance boundaries were applied to the absorbers based on their frequency-dependent electromagnetic properties. Radiation boundaries were also included in selected regions to minimize reflections and simulate open-field propagation. The proposed system of the simulation model is shown in figure 6:

To validate the accuracy of the simulation model, a comparative approach was implemented using theoretical SE calculations. Instead of relying solely on experimental data, reference values were generated using analytical models based on well-established electromagnetic shielding theory [29, 30]. This approach assesses whether the simulation model can reliably reproduce theoretical predictions.

The validation process involved defining hypothetical materials with known values of permittivity (ε_r), permeability (μ_r), and conductivity (σ).

The SE for these materials was initially computed using analytical formulas, considering both reflection loss ($\mathrm{SE_R}$) and absorption loss ($\mathrm{SE_A}$) [31],

$$\mathrm{SE_R} = 20\log\left|\frac{Z_\mathrm{m}+Z_0}{4Z_\mathrm{m}}\right| \tag{6}$$

$$Z_\mathrm{m} = \sqrt{\frac{j\omega\mu}{\sigma+j\omega\varepsilon}} \tag{7}$$

$$\mathrm{SE_A} = 8.686\alpha d \tag{8}$$

$$\alpha = R_e\left(\sqrt{j\omega\mu\left(\sigma+j\omega\varepsilon\right)}\right) \tag{9}$$

where Z_0 is the impedance of free space, typically 377 Ω, Z_m is the intrinsic impedance of the material, α is the attenuation constant and d is the thickness of the shielding material.

The total SE can be expressed as:

$$\mathrm{SE_{total}} = \mathrm{SE_R} + \mathrm{SE_A}. \tag{10}$$

The developed simulation model for the SE analysis of the Absorber Box method is shown in figure 7:

After obtaining theoretical SE values, the same material parameters were implemented in the simulation environment, ensuring that boundary conditions and material properties were consistent with the analytical model. As established in previous sections, the simulations were conducted using 30 × 30 cm samples, based on the conclusions drawn earlier regarding optimal sample dimensions.

Figure 8 illustrates the general trend of SE values between the two approaches: theoretical and simulated. The trends are well-aligned, particularly at mid-frequencies and the minor deviations observed at higher frequencies suggest potential

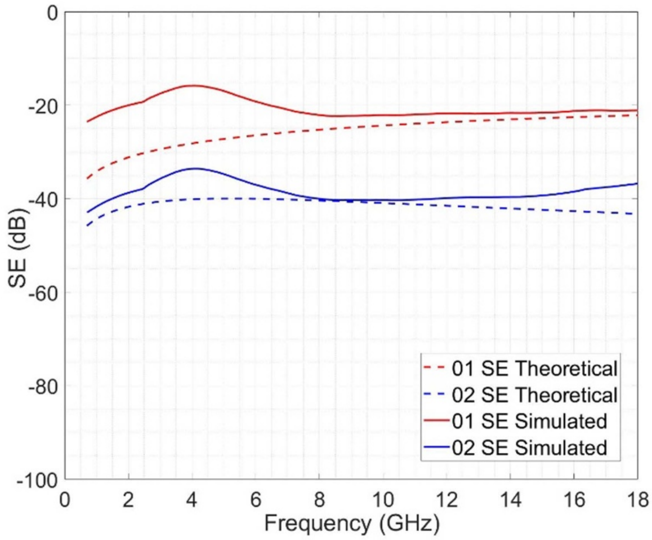

Figure 8. Comparison of theoretical and simulated S_{21} parameters for materials with different conductivities.

Table 1. Comparison of the theoretical and simulated values of the hypothetical materials.

ID	Theoretical value @1 GHz	Simulated value @1 GHz	Theoretical value @10 GHz	Simulated value @10 GHz
01	–34.17 dB	–22.34 dB	–24.33 dB	–22.11 dB
02	–44.32 dB	–41.51 dB	–40.92 dB	–40.27 dB

numerical approximations or limitations in wave interactions within the simulation environment. The discrepancies between theoretical and simulated SE values become more pronounced at lower frequencies, particularly below 7–8 GHz. This effect can be attributed to the findings presented in figure 5, which demonstrate that the SE of smaller samples is significantly affected by diffraction effects in this frequency range. Additionally, the simulation model has intrinsic limitations that become more evident at lower frequencies, where the cavity dimensions influence the accuracy of the computed SE values.

The results of the simulations are compared with the theoretical calculations to evaluate their agreement in table 1.

The results confirm that the simulation model can replicate the shielding behavior predicted by theoretical models, particularly at mid and high frequencies, where both approaches exhibit great agreement. At lower frequencies, the simulated SE values tend to underestimate the theoretical predictions. Despite these differences, the overall correlation between theoretical and simulated values supports the reliability of the simulation model. It is worth noting that the strong agreement observed at higher frequencies, where the wavelength is comparable to or smaller than the structural features of the system, validates the accuracy of the simulation geometry, material modeling and boundary conditions. This consistency confirms that the digital twin developed using FEM can be used not only to interpret experimental results, but also to optimize the design of future measurement setups and to pre-assess the performance of new materials under similar conditions. Therefore, the simulation model serves as a robust predictive tool, extending the applicability of the Absorber Box methodology to a wider range of configurations and frequency bands.

4. Results and discussion

This section presents the results of the transmission and SE assessment, along with the analysis of the electric field distribution in the tested materials. Initially, the measurement system and numerical model are validated through a comparative analysis of the S_{21} scattering parameter in free space. Subsequently, the SE of various materials is quantified to establish their attenuation characteristics.

Furthermore, the *E*-field distribution is analyzed to provide deeper insight into the interaction between electromagnetic waves and the shielding materials. This evaluation enables the identification of localized variations in field intensity, offering a more comprehensive understanding of attenuation efficiency and shielding performance across different materials.

4.1. Transmission and SE results

The first step in validating the system involved analyzing the accuracy of the reference measurement ($S21_{air}$), which serves as a baseline for comparison with the tested materials. This measurement is crucial, as a considerable discrepancy between the experimental and simulated values in the absence of a sample could indicate errors in the system setup or equipment calibration. The comparison of $S21_{air}$ presented in figure 9 exhibited a strong correlation between the simulation model

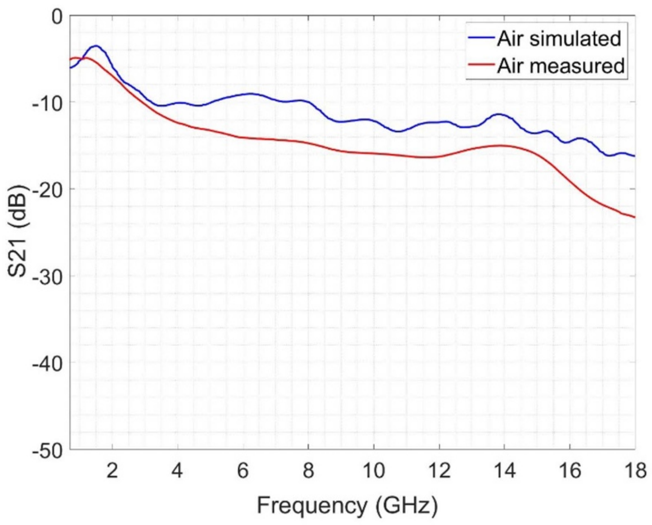

Figure 9. Comparison of the S_{21} parameter of the air obtained by FEM simulation and experimentally measured.

and the experimental data, with both following similar trends and closely matching the measured traces across the analyzed frequency range.

While a significant agreement is observed, some differences between the simulation and experimental results are expected due to the inherent complexity of accurately replicating all elements of the physical setup in a numerical model. To further investigate these variations and enhance the understanding of the measurement system, a more detailed analysis is conducted using an alternative material.

Figure 10 presents a comparative analysis of two graphs: the first illustrates the measured S_{21} parameter for a dielectric material ($\sigma = 0$, $\mu \approx 1$ and $\varepsilon \approx 19$). In contrast, the second depicts the SE, calculated as the difference between the material's S_{21} measurement and the air reference. It is observed that the agreement between measured and simulated traces is less pronounced in the S_{21} graph (figure 10(a)), primarily due to approximations in the simulation model. These discrepancies stem from the inherent tolerances in the characterization of the absorber material, as well as the complexity associated with accurately replicating the antenna model, particularly in terms of radiation pattern and gain. However, when the air reference is subtracted (figure 10(b)), the resulting SE traces exhibit a significantly improved correspondence between measured and simulated data. Given that SE is the key parameter for evaluating electromagnetic shielding performance, the strong agreement in the SE graph provides validation for the accuracy and reliability of the simulation model across the analyzed frequency range.

In figure 10(a), the agreement between simulation and experiment is strongest below 4 GHz, with the traces closely matching, particularly at 2.7 GHz, where both take a value of -10.23 dB. However, as frequency increases, the measured transmission tends to be lower than the simulated data, with the most significant discrepancies occurring above 12 GHz. The largest error is found at the 18 GHz frequency, where the difference between the measured and simulated traces is

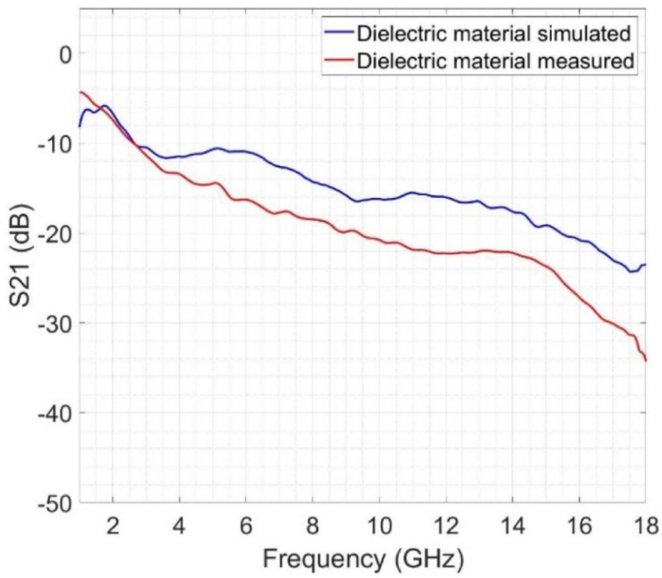

(a)

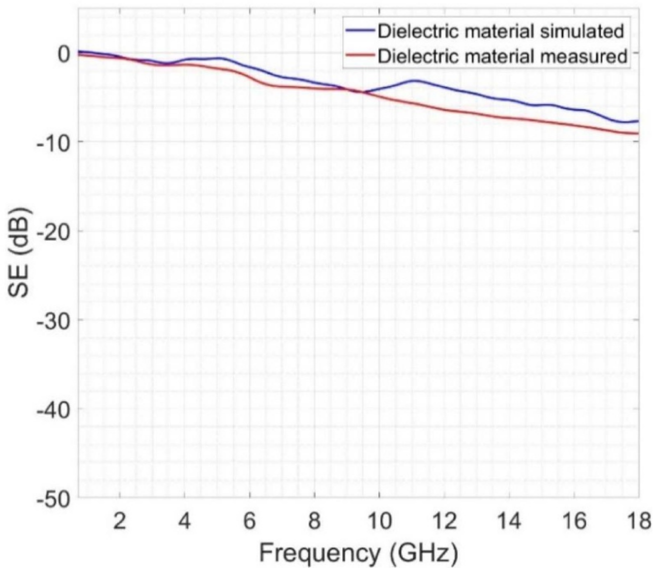

(b)

Figure 10. Comparison of the measurements of a dielectric material obtained by FEM simulation and experimentally measured. (a) S_{21} (dB); (b) SE (dB).

-10.8 dB, primarily attributed to variations in the dielectric properties of the real sample, additional losses introduced by the experimental setup, or simplifications in the antenna radiation pattern and cable transitions not fully captured in the model. On the other hand, in figure 10(b), the agreement between the two traces is more pronounced at lower frequencies, particularly below 4 GHz. In this case, the largest error is found at the 11.1 GHz frequency, being 2.5 dB, likely associated with residual cavity effects or small imperfections in the absorber performance at higher frequencies.

After confirming the agreement between simulated and experimental results, measurements were conducted on a set of selected materials with different attenuation levels (figure 11).

Table 2. Sample description.

Sample ID	Description	Dimensions (mm)
Composite material	Glass fiber reinforced composite with 3%wt of carbon nanotubes	30 × 30 × 21
Dielectric material	High-performance dielectric material	30 × 30 × 6.0
Shielding textile	Conductive shielding fabric	30 × 30 × 0.1
Absorber sheet 01	Flexible electromagnetic absorber sheet	30 × 30 × 1.0
Absorber sheet 02	Flexible electromagnetic absorber sheet	30 × 30 × 2.0
Thermal-shielding material 01	Thermally and electromagnetic shielding material	30 × 30 × 1.0
Thermal-shielding material 02	Thermally and electromagnetic shielding material	30 × 30 × 3.0

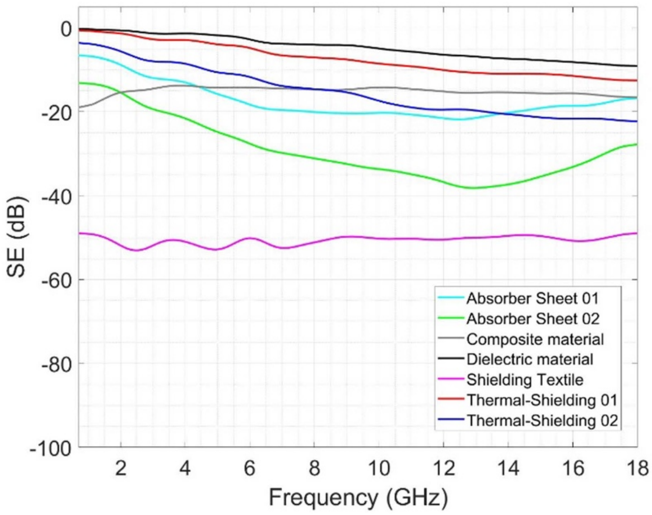

Figure 11. Experimental SE results for the different samples, measured using the Absorber Box method.

The materials were chosen to represent a wide range of SE, from low to high attenuation, ensuring a comprehensive evaluation of the Absorber Box measurement system under various shielding conditions. The analyzed samples included a glass fiber-reinforced composite with 3%wt carbon nanotubes, a high-performance dielectric material, a conductive shielding fabric, a flexible electromagnetic absorber sheet in two different thicknesses, and a thermally and electromagnetically shielding material, also tested in two thicknesses. Each of these materials exhibits distinct electromagnetic properties and various levels of attenuation. All of the samples are described in table 2.

The glass fiber-reinforced composite with 3%wt carbon nanotubes is expected to provide moderate attenuation, as the conductive fillers within the insulating matrix contribute to partial electromagnetic wave absorption and reflection. The high-performance dielectric material, being non-conductive, is anticipated to exhibit minimal SE, primarily affecting wave propagation rather than absorption or reflection. The flexible electromagnetic absorber sheets, tested in two different thicknesses, are specifically engineered for absorption, with greater attenuation expected for the thicker variant. Similarly, the thermal–electromagnetic shielding materials, also evaluated in two thicknesses, combine thermal insulation with electromagnetic shielding, with the thicker sample expected to provide enhanced attenuation. The conductive shielding fabric is designed for lightweight EMI protection, offering higher attenuation than the other materials due to its conductive nature. By analyzing these materials, this study aims to evaluate the Absorber Box's ability to differentiate between varying shielding capabilities and validate its performance across a diverse set of shielding materials.

Experimental results indicated that materials with higher conductivity exhibited significantly greater SE values, with attenuation levels exceeding −50 dB across the measured frequency range. In contrast, materials with lower conductivity provided a more moderate or negligible reduction in EMI. The most notable trend is observed in the shielding textile, which consistently maintains the highest attenuation, with SE values below −50 dB across the entire frequency range, confirming its efficiency as an EMI shielding material primarily due to strong reflection mechanisms.

The glass fiber-reinforced composite with 3%wt carbon nanotubes shows a gradual decrease in SE with increasing frequency, ranging from approximately −10 dB at low frequencies to nearly −30 dB at higher frequencies. This suggests that while the presence of carbon nanotubes enhances shielding performance, the material does not act as a perfect barrier, likely due to its composite structure and partial conductivity. In contrast, the dielectric material demonstrates negligible SE, remaining close to 0 dB in the low frequency range, reinforcing its expected role in wave propagation rather than attenuation.

A frequency-dependent behavior is evident in the flexible electromagnetic absorber sheets, where Absorber Sheet 02 (thicker variant) outperforms Absorber Sheet 01, particularly above 8 GHz, where their SE values diverge more significantly. This suggests that absorption mechanisms in these materials become more effective at higher frequencies. A similar frequency-dependent trend is observed in the thermal–electromagnetic shielding materials, where Thermal-Shielding 02 exhibits slightly higher attenuation than Thermal-Shielding 01, particularly in the mid-frequency range (6–12 GHz). However, both thermal shielding materials show less attenuation compared to the absorber sheets, indicating a combined but less dominant shielding mechanism. An interesting behavior is seen in the composite material and thermal-shielding traces, which show a clear dip in attenuation around 8–12 GHz, suggesting possible resonance effects or

Table 3. SE values of the different samples.

Sample ID	SE value @1 GHz	SE value @10 GHz
Composite material	−18.51 dB	−14.19 dB
Dielectric material	−0.31 dB	−4.92 dB
Shielding textile	−49.10 dB	−50.23 dB
Absorber sheet 01	−6.74 dB	−20.26 dB
Absorber sheet 02	−13.29 dB	−33.67 dB
Thermal-shielding material 01	−0.71 dB	−8.51 dB
Thermal-shielding material 02	−3.81 dB	−17.39 dB

frequency-dependent interactions within their structures. In contrast, the shielding textile remains nearly constant, suggesting a broadband shielding response with minimal frequency-dependent variations.

Table 3 summarizes the shielding effectiveness values of all tested materials at 1 GHz and 10 GHz.

Overall, these results emphasize the strong reflective shielding capabilities of conductive textiles, the frequency-dependent nature of absorbers, and the limitations of dielectric and composite materials in providing significant shielding. The findings highlight the importance of selecting shielding materials based on the specific frequency range and required attenuation levels for EMI protection applications. Furthermore, the absorber-based measurement system demonstrates high resolution in distinguishing SE variations across different materials and frequency ranges. Its ability to precisely discern differences in attenuation mechanisms reinforces its reliability for comprehensive SE characterization in diverse shielding applications.

4.2. Electric field distribution results

To further validate the accuracy of the measurement system, simulations were performed to analyze the distribution of the electric field within the Absorber Box method. These simulations provide a detailed analysis of the wave propagation behavior, allowing for a better understanding of how electromagnetic waves interact with the system components, including the antennas, the absorbing materials, and the samples.

Figure 12 pretends to evaluate the impact of the absorbing material on minimizing the influence of unwanted effects in the characterization of SE in the AIR reference measurement. A comparison of the *E*-field distribution in AIR is presented, with and without the presence of the absorbing material, at a frequency of 10 GHz. This frequency has been selected as a reference throughout the study to maintain consistency with previous results. Figure 12(a) illustrates the reference measurement without the absorbing material. In this setup, significant variability is observed due to reflections and disturbances caused by the environment and the measurement system configuration. These unwanted interferences affect the accuracy of the measurement and can introduce inconsistencies in SE characterization, leading to unreliable results. In contrast, figure 12(b) shows the reference measurement

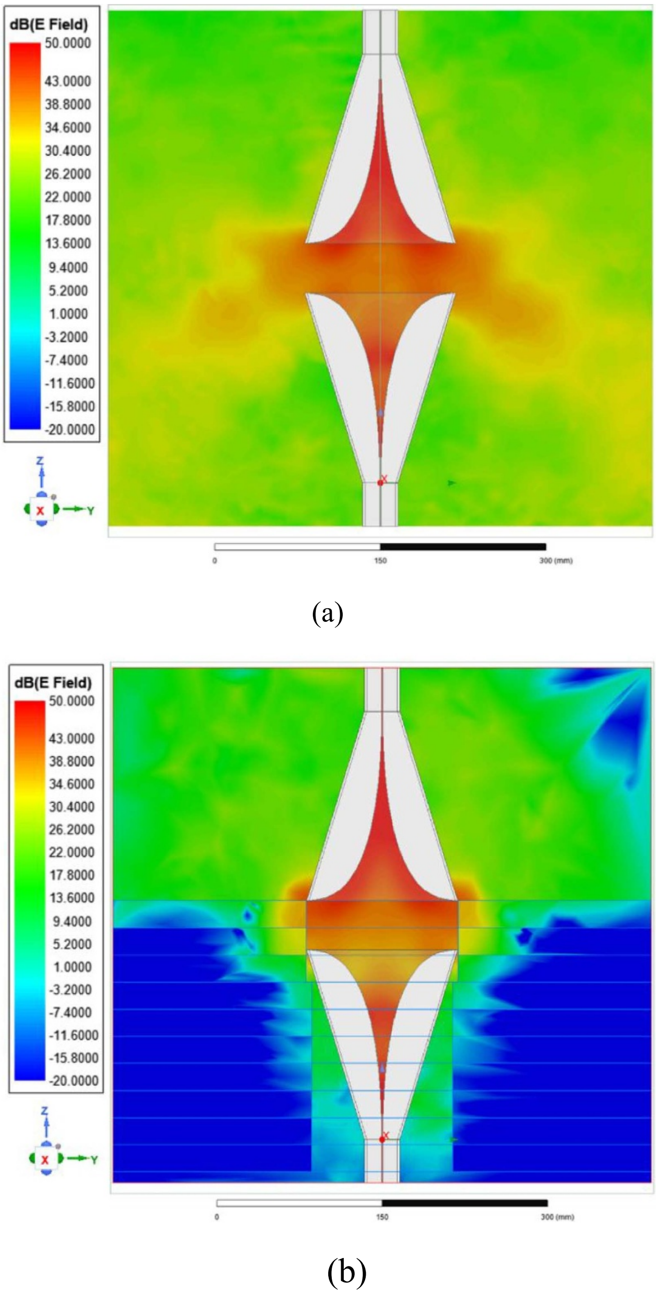

Figure 12. Analysis of the *E*-field distribution in dB. (a) The reference AIR measurement without the absorbing material; (b) the reference AIR measurement with the absorbing material.

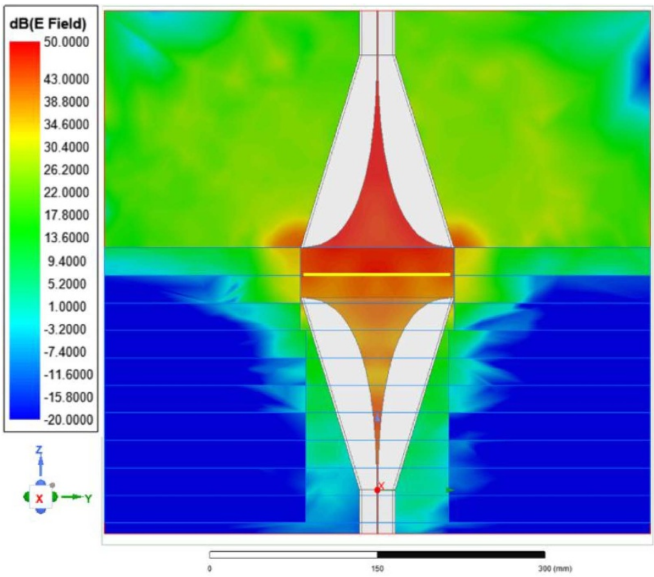

(a)

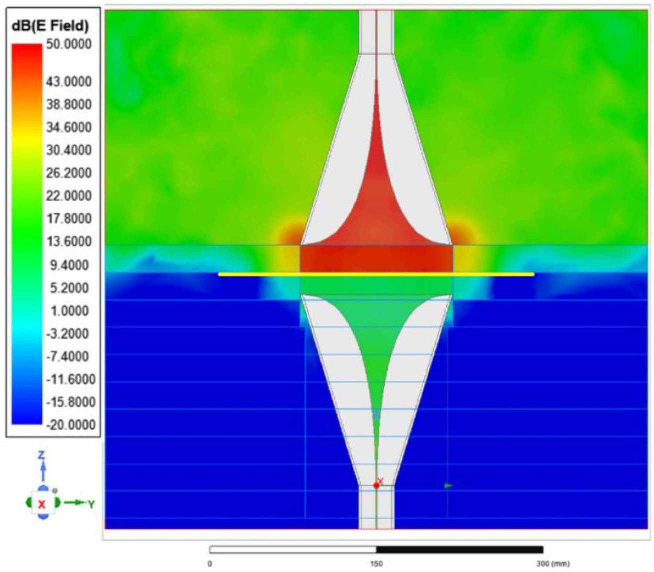

(b)

Figure 13. Analysis of the *E*-field distribution. (a) The 12 × 12 cm MUT; (b) the 30 × 30 cm MUT.

of air with the absorbing material placed inside the cavity. The absorbing material creates a controlled electromagnetic propagation channel, significantly reducing unwanted effects associated with antenna interference. The presence of the absorbing material minimizes signal distortions and effectively mitigates environmental reflections, leading to a more stable and accurate measurement of the SE baseline.

These results justify the use of the absorbing material in the measurement system, as its inclusion enables a more precise evaluation of the material's effect on electromagnetic radiation attenuation, thereby ensuring a controlled and repeatable testing environment.

On the other hand, figure 13 investigates the influence of sample size on SE characterization by comparing two samples of the previously mentioned material 02, with dimensions of 12 × 12 cm and 30 × 30 cm, respectively. This comparison allows for a clearer understanding of how the size of the sample affects the transmission of electromagnetic. Figure 13(a) depicts the field distribution for the 12 × 12 cm sample. In this case, the electromagnetic field manages to leak into the receiving antenna due to pronounced edge diffraction effects. This phenomenon results in a decrease in the measured attenuation, leading to an underestimation of the material's SE. The relatively small sample size allows a considerable portion of the incident field to bypass the material, reducing its apparent shielding performance. By contrast, figure 13(b) presents the field distribution for the 30 × 30 cm sample. With the increased sample size, the unwanted transmission through the edges is significantly reduced, ensuring a more accurate evaluation of the material. The larger sample better confines the electromagnetic field, minimizing diffraction effects and yielding a more representative measurement of the SE.

These findings align with the results presented in figure 5, which demonstrate the impact of sample size on SE measurements. As the sample size increases, edge diffraction decreases, leading to a more accurate representation of the material's intrinsic electromagnetic behavior. This analysis confirms the necessity of using appropriately sized samples to ensure reliable SE measurements and to minimize errors caused by geometric effects unrelated to the material's inherent shielding properties.

5. Conclusions

This study validated the accuracy and effectiveness of an enhanced Absorber Box method for measuring SE in electromagnetic applications. Through a combined approach of experimental, theoretical and simulation analysis, the proposed system demonstrated reliable measurements across a broad frequency range, addressing several limitations of existing standardized methods. The experimental and simulated results exhibited strong overall agreement, supporting the reliability of the proposed model. However, minor discrepancies were identified in specific spectral regions that can be attributed to the interaction between sample geometry and the electromagnetic field distribution within the Absorber Box, as well as localized interference and resonance effects.

A key finding of this study was the significant influence of sample size on SE measurements. It was observed that smaller samples exhibited stronger edge diffraction effects, which could lead to an underestimation of the material's true attenuation capabilities. Conversely, appropriately sized samples minimized these diffraction effects, resulting in more precise and representative measurements.

Additionally, the inclusion of absorbing material within the measurement box significantly enhanced system accuracy by reducing unwanted interferences and minimizing internal reflections. This optimized design enabled the effective characterization of a wide range of shielding materials. The experimental results confirmed the system's capability to differentiate materials with varying attenuation levels, demonstrating its precision and reliability in distinguishing SE across different materials and frequency ranges. The ability to accurately measure materials with different shielding performances reinforces the robustness of this method as a practical alternative to conventional SE measurement techniques.

In conclusion, the proposed method represents an efficient and flexible alternative for the characterization of electromagnetic shielding materials. Its combination of accuracy, ease of implementation, and compatibility with diverse materials makes it a valuable tool for applications in telecommunications, automotive, aerospace, and other sectors where EMI is a critical concern. Future research may focus on optimizing the box geometry and analyzing materials with more complex properties to further enhance the system's precision and applicability.

Data availability statement

No new data were created or analysed in this study.

Acknowledgments

This study forms part of the Advanced Materials programme and was supported by MCIN with funding from European Union NextGenerationEU (PRTR-C17.I1) and by Generalitat Valenciana (MFA/2022/060).

References

[1] Min Koo C, Sambyal P, Iqbal A, Shahzad F and Hong J 2021 Electromagnetic interference and shielding *Two-Dimensional Materials for Electromagnetic Shielding* (Wiley) pp 1–24
[2] Vance E F and Graf W 1988 The role of shielding in interference control *IEEE Trans. Electromagn. Compat.* **30** 294–7
[3] Futatsumori S and Hiraga N 2024 Electromagnetic interference issues of aircraft radio altimeters due to Sub-6 band 5G mobile communications systems in Japan *2024 IEEE Joint Int. Symp. on Electromagnetic Compatibility, Signal & Power Integrity: EMC Japan/Asia-Pacific Int. Symp. on Electromagnetic Compatibility (EMC Japan/APEMC Okinawa)* (IEEE) pp 45–48
[4] Son H and Chong Y 2019 Analysis of the interference effects of 5G system on automotive collision avoidance radars *2019 Int. Conf. on Information and Communication Technology Convergence (ICTC)* (IEEE) pp 1463–6
[5] Gallardo B P, de Francisco P G, Romero S F, Rebate I M, Somolinos D R and Martinez D P 2021 Limitations in the shielding effectiveness measurement methods for carbon fiber composites *IEEE Electromagn. Compat. Mag.* **10** 52–61
[6] ASTM standard (ASTM D4935-18) 2018 *Test Method for Measuring the Electromagnetic Shielding Effectiveness of Planar Materials* (https://doi.org/10.1520/D4935-18)
[7] Anon 2007 IEEE standard method for measuring the effectiveness of electromagnetic shielding enclosures *IEEE Std 299-2006 (Revision of IEEE Std 299-1997)* pp 1–52
[8] Micheli D, Delfini A, Pastore R, Marchetti M, Diana R and Gradoni G 2017 Absorption cross section of building materials at mm wavelength in a reverberation chamber *Meas. Sci. Technol.* **28** 024001
[9] David N A, Wild P M and Djilali N 2012 Parametric study of a polymer-coated fibre-optic humidity sensor *Meas. Sci. Technol.* **23** 035103
[10] Bakli H, Moualhi M and Makhlouf M 2022 High-sensitivity electrical properties measurement of graphene-based composites using interferometric near-field microwave technique *Meas. Sci. Technol.* **33** 045012
[11] Qiu L, Ding S, Wang D and Han B 2023 Self-sensing GFRP-reinforced concrete beams containing carbon nanotube-nano carbon black composite fillers *Meas. Sci. Technol.* **34** 084003
[12] Chang T, Zhang X, Yang C, Sun Z and Cui H-L 2017 Measurement of complex terahertz dielectric properties of polymers using an improved free-space technique *Meas. Sci. Technol.* **28** 045002
[13] Amaro A, Suarez A, Tamburrano A, Torres J, Marra F, Martinez P A, Galindo B, Soriano N, Victoria J and Alcarria A 2023 EMI shielding effectiveness study for innovative carbon nanotube materials in the 5G frequency region *IEEE Trans. Electromagn. Compat.* **65** 177–85
[14] Martinez P A, Victoria J, Torres J, Suarez A, Alcarria A, Amaro A, Galindo-Galiana B, Losada-Fernandez C, Ramirez-Monsell V and Lopez-Rius B 2021 Analysis of EMI shielding effectiveness for plastic fiber composites in the 5G sub-6 GHz band *2021 Joint IEEE Int. Symp. on Electromagnetic Compatibility Signal and Power Integrity, and EMC Europe, EMC/SI/PI/EMC Europe 2021*
[15] Barjola A, Herráiz R, Amaro A, Torres J, Suárez A and Giménez E 2024 $Ti_3C_2T_x$ electromagnetic shielding performance: investigating environmental influences and structural changes *Adv. Electron. Mater.* **10** 2400024
[16] Zapata A S, Dawson J F, Ariën Y, Catrysse J, Pissoort D and Marvin A C 2023 An overview of the IEEE P2715 guide for the characterization of the shielding effectiveness of planar materials *IEEE Electromagn. Compat. Mag.* **12** 78–88
[17] 2023 *IEEE Std 2715™ Guide for the Characterization of the Shielding Effectiveness of Planar Materials* IEEE Standard
[18] Marvin A C, Dawson L, Flintoft I D and Dawson J F 2009 A method for the measurement of shielding effectiveness of planar samples requiring no sample edge preparation or contact *IEEE Trans. Electromagn. Compat.* **51** 255–62
[19] Amaro A, Suarez A, Torres J, Martinez P A, Herraiz R, Alcarria A, Benedito A, Ruiz R, Galvez P and Penades A 2023 Shielding effectiveness measurement method for planar nanomaterial samples based on CNT materials up to 18 GHz *Magnetochemistry* **9** 114
[20] Brown T W C and Khalily M 2018 Integrated shield edge diffraction model for narrow obstructing objects *IEEE Trans. Antennas Propag.* **66** 6588–95
[21] Kang J-S, Kim J-H and Park J-I Reduction of edge diffraction effects of MUT holder using EM absorber in W-band free-space material measurements
[22] Yingpeng F, Zhengwei D, Gong K and Guoding L 2003 Analysis on shielding effectiveness of metallic enclosures with slot *Asia-Pacific Conf. on Environmental*

Electromagnetics, 2003. CEEM 2003. Proc. (IEEE) pp 43–46
[23] Anon datablad-TFAL series. Electromagnetic Absorber Datasheet
[24] Balanis C A Antenna theory analysis and design third edition
[25] Paknys R 2016 Uniform theory of diffraction *Applied Frequency-Domain Electromagnetics* (Wiley) pp 268–316
[26] Kandimalla D, De A and Sanyal S 2015 A novel UTD-type diffraction coefficient for a straight edge in a curved screen *IEEE Trans. Antennas Propag.* **63** 1172–7
[27] Keller J B Geometrical theory of diffraction*
[28] Kouyoumjian R G and Pathak P H 1974 A uniform geometrical theory of diffraction for an edge in a perfectly conducting surface *Proc. IEEE* **62** 1448–61
[29] Schelkunoff S A 1943 *Electromagnetic Waves* (D Van Nostrand)
[30] McDowell A J and Hubing T H 2014 Analysis and comparison of plane wave shielding effectiveness decompositions *IEEE Trans. Electromagn. Compat.* **56** 1711–4
[31] Ott H W 2009 *Electromagnetic Compatibility Engineering* (Wiley)